Measurement of the Ionization State and Electron Temperature of Plasma during the Ablation Stage of a Wire-Array Z Pinch Using Absorption Spectroscopy

V. V. Ivanov,[1] P. Hakel,[1] R. C. Mancini,[1] J. P. Chittenden,[2] A. Anderson,[1] T. Durmaz,[1] P. Wiewior,[1] D. Papp,[1] S. D. Altemara,[1] A. L. Astanovitskiy,[1] and O. Chalyy[1]

[1]*Department of Physics, University of Nevada, Reno, Nevada 89557, USA*
[2]*Blackett Laboratory, Imperial College, London SW7 2BZ, United Kingdom*

(Received 10 January 2011; published 2 June 2011)

Wire-array plasmas were investigated in the nonradiative ablation stage via x-ray absorption spectroscopy. A laser-produced Sm plasma was used to backlight Al wire arrays. The Sm spectrum was simultaneously observed by two spectrometers: one recorded the unattenuated spectrum and the other the transmission spectrum with 1.45–1.55 keV K-shell absorption lines. Analysis of absorption spectra revealed electron temperature in the range of 10–30 eV and the presence of F-, O-, N- and C-like Al ions in the absorbing plasma. A comparison of this electron temperature with the postprocessed absorption spectra of a 2D MHD simulation yields results in general agreement with the data analysis.

DOI: 10.1103/PhysRevLett.106.225005 PACS numbers: 52.59.Qy, 52.70.La

Wire-array Z pinches are the most powerful and efficient laboratory sources of x-ray radiation [1,2]. X-ray spectroscopy is the main method for diagnosing stagnated Z-pinch plasmas using K-shell and M-shell x-ray emission spectra [3–5]. Wire-array Z pinches go through ablation, implosion, and stagnation phases [6]. The behavior of wire-array plasmas in the ablation and early implosion stages predetermines the formation of the pinch and is responsible for their radiative properties at the stagnation stage. However, plasma conditions at these early stages cannot be determined with K-shell emission spectroscopy. In this work we studied the ionization and temperature of wire-array plasmas in the nonradiative stage using x-ray absorption spectroscopy.

Absorption spectroscopy has been a powerful tool for investigation of laser-produced plasmas [7–9]. Also, it has been used to measure Fe opacity at conditions relevant for solar physics [10]. X pinches and laser-produced plasma have been used for narrowband backlighting of wire arrays [11–13], and X pinches have been suggested for absorption spectroscopy [14]. The main difficulty in using x-ray absorption spectroscopy with a laser-driven backlight source in Z pinch experiments is to overcome the intense burst of x-rays emitted at the collapse of the Z pinch. Z pinches at the 1-MA Zebra facility generate x-ray bursts with 5–25 kJ of total energy, of which 0.5–1 kJ is in the keV photon-energy range [15]. Furthermore, these x rays produce an x-ray fluorescence effect in the vacuum chamber that can compromise absorption measurements.

In this Letter we report the first successful application of x-ray absorption spectroscopy to wire-array Z-pinch plasmas during the ablation stage. To this end, a 50-TW laser [16] was coupled to a 2-TW pulsed power generator, and served as the driver of a Sm source of x-ray photons to probe 18-wire star Al wire-arrays Z-pinch plasmas [17] via absorption spectroscopy.

The experiments were carried out at the Nevada Terawatt Facility (NTF). The Zebra generator produced a 1-MA current pulse with a rising edge of ~80 ns (10%–90%). The Leopard laser was used to illuminate a Sm foil, whose M-shell x-ray emission served as the backlighter for the wire-array Al plasma. Leopard [16] delivered a 0.8-ns, 8.6 cm diameter, 12–18 J laser pulse which was focused to a 25-micron diameter spot on the Sm target in the Zebra vacuum chamber with an intensity of $(0.8–1.2) \times 10^{15}$ W/cm^2 and a contrast ratio of 10^6. In preparation for the experiments, Al $1s$-$2p$ absorption lines in the range of 1.45–1.55 keV were modeled for wire-array plasmas in the ablation stage with electron temperature from 10 to 50 eV. The calculations were performed with the collisional-radiative atomic kinetics codes PRISMSPECT [18] and ATOKIN. Figure 1 presents synthetic transmission spectra calculated for a slab Al plasma with electron temperatures $T_e = 20$ and 40 eV, ion density $N_i = 2 \times 10^{19}$ cm^{-3}, and length $L = 0.4$ mm. We note that K-shell absorption lines in Al plasmas with electron temperature $T_e = 5–50$ eV and K-shell emission lines of stagnated Z-pinch plasma with $T_e = 300–400$ eV are located in different spectral regions.

Figure 2 displays the experimental setup. The load is installed in the return current cage of 8 cm in diameter. Aluminum alloy 5056 with 5% of Mg was used as load material. We checked that Mg K-shell absorption lines do not interfere with Al absorption spectra for our plasma conditions. Plasmas produced with 3-leg star wire arrays [15] with a total of 18 wires, each wire with a diameter of 12.7 μm, and located at diameters of 20/18.5/17/15.5/14/6 mm were studied at the ablation stage. These Zebra Al star wire arrays radiate 6.5–7.5 kJ of total x-ray energy. During the ablation stage, the wires remain at their initial positions due to the "core-corona" structure of plasma columns [6,19] while ablated material streams

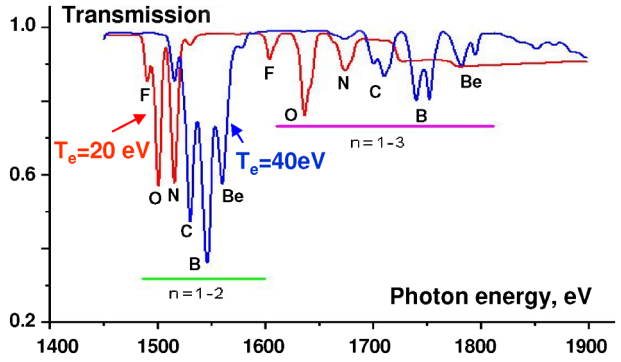

FIG. 1 (color online). Synthetic Al K-shell transmission spectra of Al plasma with $T_e = 20$ and 40 eV in the range of 1.45–1.55 keV calculated with a detailed collisional-radiative atomic kinetics and spectral code, including the effect of instrumental resolution of $E/dE = 300$.

from the wires to the center of the array. The implosion phase starts when breaks appear on the wire cores and the plasma is accelerated inwards to the array center [20]. In star wire arrays the implosion stage begins with the outer wires and then cascades to the center [17].

Broadband x-ray radiation from a 25 μm thick Sm foil irradiated by the Leopard laser was recorded by two time-integrated conical spectrometers [21] with a cone angle of 12°. Given the brightness of the backlit photon's source, focusing spectrometers were needed to provide enough sensitivity at a distance of 15 cm from the laser target to the crystal. Mica crystal was selected for spectrometers to mitigate the after-shot shock effect in Zebra. Spectra were recorded on BioMax x-ray film [22]. The resolution power of conical spectrometers with mica crystals in the first order was 250–300. Spectrometer S1 recorded the transmission of the backlighter through one leg of the star wire

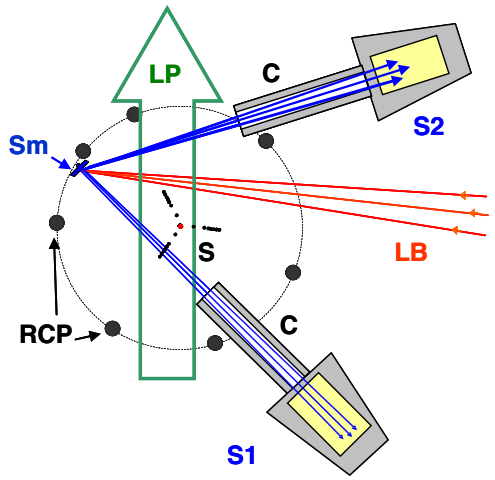

FIG. 2 (color online). Experimental setup. S1 and S2—conical x-ray spectrometers with mica crystals; C—collimators; LB—a Leopard laser beam at the wavelength of 1056 nm; S—a 3-ray star wire array; Sm—samarium laser target; LB—laser probing beam at the wavelength of 532 nm; RCP—return current posts.

array, and spectrometer S2 recorded the unattenuated backlighter radiation needed to interpret the transmission spectrum. X-ray radiation was filtered by 2 μm polycarbonate films located on the front end of the spectrometers and by 8 μm mylar films with 0.3 μm Al layers on the film cassette. The spectrometers were installed on damping tables and shielded against the primary x-ray radiation and secondary x-ray fluorescence. Spectral calibration of spectrometers was done in their working positions in the Zebra vacuum chamber using Mg and Al K-shell lines from laser-produced plasmas in calibration shots. We estimate that the electron temperature of the plasma backlighter is in the range $T_e = 200$–250 eV and the contribution to Sm spectra from higher-order reflection in the Mica crystal is negligible at this electron plasma temperature. Samarium $4f$-$3d$ lines were identified in the quasicontinuum spectra using simulations and spectral calibration [23] from a laser-produced plasma. X-ray spectrometers were aligned on the focal spot of the Leopard laser by using alignment cw lasers fielded on axes of spectrometers. Alignment was controlled with a long-distance microscope.

The backlighting pulse was timed to probe the ablation stage which lasts 50–55 ns in star wire arrays. Since the ablating plasma columns remain near the wire's initial positions, the bright x-ray emission from the stagnated Z-pinch later in time was blocked with collimators (see Fig. 2). Two-frame shadowgraphy at a wavelength of 532 nm was also used to diagnose the wire-array plasma conditions during the x-ray backlighting and identify the beginning of the implosion stage. The first frame was timed to the Leopard laser pulse and the second frame 25 ns later. Figure 3 shows typical shadowgrams (a) and (b), and directions of optical and x-ray probing (c). The first frame (a) presents the ablation stage and the second frame (b) shows the beginning of the bubblelike implosion [20]. The rectangular area marked in the shadowgram (a) identifies the backlit area on the wire array. Figure 3(e) shows good shot-to-shot reproducibility of the Sm spectrum. A structure in the spectrum of Fig. 3(e) correlates with Sm spectra in [23] and was used for spectral calibration. The dip in the spectral intensity at the wavelength of 7.95 Å is associated with a reduction of reflectivity of the mica crystal near the Al K-edge absorption. A laser-only reference shot was performed before every coupled laser-Z-pinch shot. After the reference shot the focal spot of the laser beam was realigned on a new portion of the Sm target for the Leopard-Zebra coupled shot. As a result, four spectra were recorded with the two spectrometers including three reference spectra and one absorption spectrum. Spectral intensities of the background radiation were subtracted from intensities of spectra. Two spectra from one spectrometer were normalized for intensity and compared. The spectrometer S2 recorded shot-to-shot spectral variations in the backlighter spectrum. Spectra in S1 and S2 spectrometers may differ due to the opacity effect in the plasma plume. Only two spectra from S1 spectrometer were used

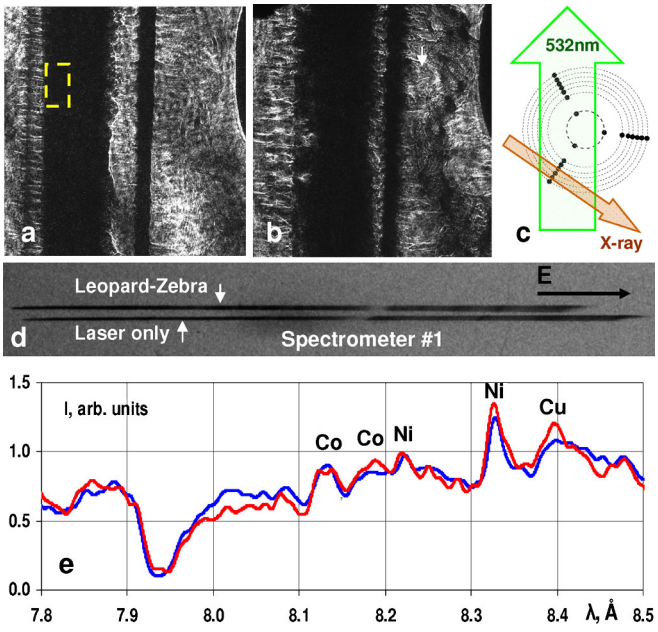

FIG. 3 (color online). (a),(b) Shadowgrams of the Al star wire array, shot 2204, during the backlighting pulse (a) and 25 ns later (b). (c) Directions of optical and x-ray probing. (d) Reference spectrum of the Sm backlighter from the laser-only shot (bottom line) and spectrum from coupled Leopard-Zebra shot 2204 (top line) in spectrometer S1. (e) Reproducibility of spectra of the Sm backlighter in two laser-only shots, spectrometer S1.

for calculation of transmission spectra in the wire-array plasma. The reference spectrometer S2 was used to monitor shot-to-shot reproducibility and for correlating x-ray intensity levels in reference and coupled shots.

Figure 4 shows the transmission spectrum averaged over two shots and model fits with one- and two-temperature models. The lines of sight cover a width of 1.1 mm in the horizontal direction, noted with a dashed box in Fig. 3(a), and include "corona" plasma of two wires and jets of ablating plasma between wires. The observed K-shell absorption lines are due to $1s$-$2p$ transitions arising from ground and low-excited states in F, O, N, and C-like Al ions. A single-temperature plasma model cannot fit the transmission spectrum (dashed line in Fig. 4). The data indicate a temperature distribution in wire-array plasma at the ablation stage in the range of 10–30 eV for an ion density of 2×10^{19} cm^{-3}. The data can be modeled with two effective electron temperatures of $T_e = 14$ and 30 eV, as shown in Fig. 4. The areal density extracted from the analysis of the transmission spectrum is 1.4×10^{18} cm^{-2} of which 84% is associated with the plasma at 14 eV and 16% at 30 eV. Thus, the lower temperature plasma dominates the formation of the transmission spectrum but a higher-temperature region is needed to accommodate the C-like feature. We note that the areal density extracted from the data analysis does not include contributions from regions of the plasma not involved in the formation of the absorption spectrum. An independent estimation of the total areal density based on the shadowgram data yields

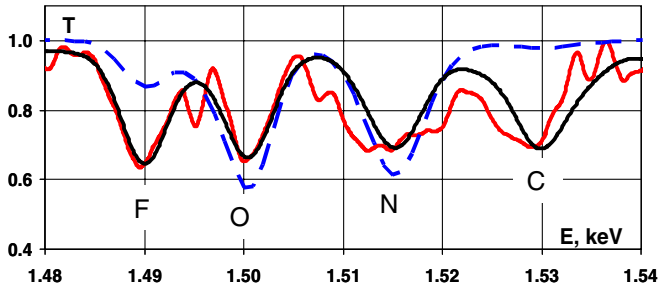

FIG. 4 (color online). Experimental transmission spectrum of ablating plasma (red or gray line) with one-temperature modeling of plasma absorption (blue dashed line) $T_e = 20$ eV, and two-temperature (black solid line) $T_e = 14$ and 30 eV.

a value in the range of (2–3) $\times 10^{18}$ cm^{-2}, thus suggesting that a large fraction of the plasma has significant population of F-, O-, N- and/or C-like Al ions and contributes to the features in the absorption spectrum. The analysis of other data sets yielded comparable results: electron temperature of the cold component in the range of 14–15 eV and the hotter component in the range of 26–30 eV. Shot-to-shot reproducibility and processing the Sm spectra are the main sources of experimental uncertainties.

The ablation stage in the Al star wire array was modeled with the 3D resistive MHD code GORGON [24]. For this work the code was run in 2D (x, y) geometry with 20 μm spatial resolution. Figure 5 displays Gorgon's 2D simulation of the distribution of mass density (a) and electron temperature (b) in the Al star wire array used in experiments at the time of the transmission measurement, i.e., 58 ns after the beginning of the current, when it has reached a value of 0.68 MA. The electron temperature spatial distribution shows $T_e = 10$–20 eV near plasma columns and $T_e = 30$–60 eV in the ablating plasma jets. The region of the wire array closer to the axis is hotter; however, this temperature increase is less pronounced in 3D simulations and it lies outside the region probed with laser shadowgram and x-ray absorption spectroscopy. Only data from the middle of the wire array indicated by the dashed arrow were taken into account since this is the region probed with x-ray spectroscopy. The mass density of higher-temperature plasma in ablating jets is significantly less compared to that of plasma columns. Therefore, the low-temperature plasma columns make the main contribution to the absorption spectrum. These temperature and density spatial distributions were postprocessed with the same atomic kinetics model employed in the data analysis and the photon-energy dependent opacity used to compute the transmission spectrum of the plasma. To this end, the radiation was transported along a direction parallel to the line of sight one photon energy at a time for a set of chords that run through all fluid elements in Gorgon's simulation. The result was convolved with the instrumental function and then analyzed as if it were data [see Fig. 5(c)]. The postprocessed transmission spectrum is dominated by F-, O-, and N-like Al ions. Again, a two-temperature effective

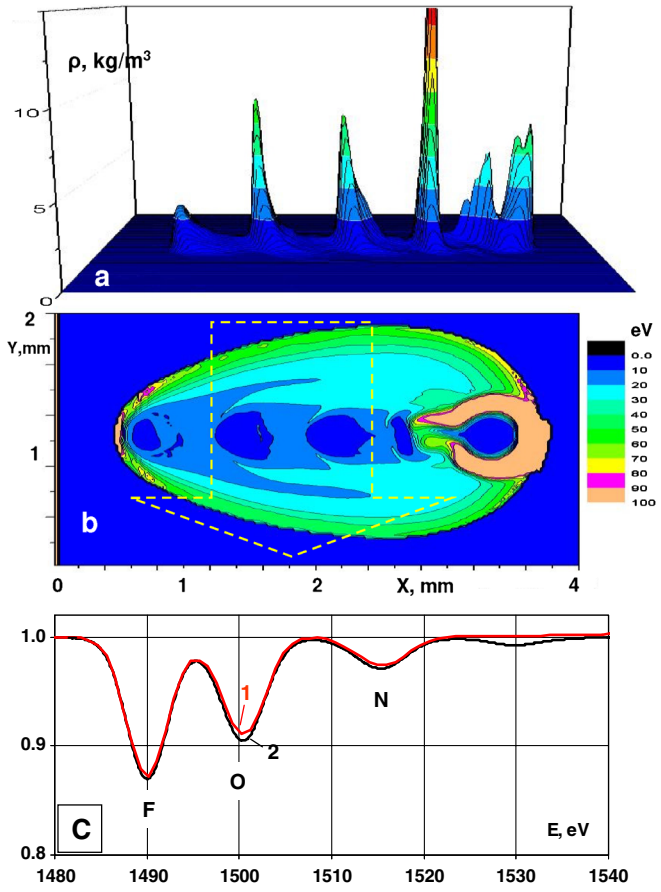

FIG. 5 (color online). 2D Gorgon simulation of the distribution of mass density and temperature in the Al star wire array at the ablation stage, 58 ns after the beginning of the current pulse: (a) mass density and (b) and electron temperature in one leg of the star wire array. The arrow represents the region probed with absorption spectroscopy. (c) The postprocessed transmission of Gorgon (1) and two-temperature model fit (2). The right-hand side is the side closest to the array center.

model was required to fit the transmission spectrum, with electron temperatures of 15 and 27 eV, and an areal-density of 1.9×10^{17} cm^{-2} of which 94% is associated with the 15 eV plasma and 6% with the 27 eV plasma. On the one hand, compared to the experiment the plasma in the simulation is characterized by a similar range of temperatures and ionization stages but the contribution from C-like Al is negligible. On the other hand, the areal density is significantly smaller and the lower temperature plasma represents an even larger fraction of it. Indeed, integration along the line of sight of the simulation's mass-density distribution within the region probed by absorption spectroscopy yielded an average value of the total areal density of 1.4×10^{18} cm^{-2}. Hence, compared to the experiment the simulation predicted that a significantly smaller amount of plasma representing only 14% of the total areal density contributed to the formation of the absorption spectrum. This is also consistent with the higher degree of transmission seen in the postprocessed, synthetic transmission spectrum compared to that in the experiment. In order to take into account the uncertainty in the location of the plasma region probed by absorption spectroscopy, the postprocessing was repeated shifting this region sideways by ± 0.1 mm. This value reflects the accuracy of alignment. This change produced negligible differences in the postprocessing analysis results.

In this work x-ray absorption spectroscopy was applied to wire-array plasmas in the ablation stage. We emphasize that the implosion phase also can be studied with this method, thus opening up both ablation and implosion phases to detailed spectroscopic studies. Upcoming experiments and analysis will employ spectrometers with increased spatial resolution to separate contributions of plasma columns and plasma jets, spectral postprocessing of Gorgon's 3D simulations, and investigation of wire arrays made out of other materials.

The authors thank A. P. Shevelko for help in experiments with laser-produced plasma, J. M. Kindel and A. M. Covington for support, and R. Presura, V. Nalajala, E. McKee, S. Batie, T. Brower, O. Dmitriev, C. Jones, and D. Macaulay for help in coupled laser-Z-pinch experiments. Work was supported by the DOE/NNSA under UNR Grant No. DE-FC52-06NA27616.

[1] T. W. L. Sanford *et al.*, Phys. Rev. Lett. **77**, 5063 (1996).
[2] C. Deeney *et al.*, Phys. Rev. Lett. **81**, 4883 (1998).
[3] J. P. Apruzese *et al.*, Phys. Plasmas **8**, 3799 (2001).
[4] J. E. Bailey *et al.*, Phys. Rev. Lett. **92**, 085002 (2004).
[5] B. Jones *et al.*, Phys. Rev. Lett. **100**, 105003 (2008).
[6] M. E. Cuneo *et al.*, Phys. Rev. E **71**, 046406 (2005).
[7] J. Bruneau *et al.*, Phys. Rev. Lett. **65**, 1435 (1990).
[8] R. Schott *et al.*, J. Quant. Spectrosc. Radiat. Transfer **81**, 441 (2003).
[9] P. Audebert *et al.*, Phys. Rev. Lett. **94**, 025004 (2005).
[10] J. E. Bailey *et al.*, Phys. Rev. Lett. **99**, 265002 (2007).
[11] D. H. Kalantar and D. A. Hammer, Phys. Rev. Lett. **71**, 3806 (1993).
[12] D. B. Sinars *et al.*, Appl. Opt. **42**, 4059 (2003).
[13] D. B. Sinars *et al.*, Phys. Rev. Lett. **93**, 145002 (2004).
[14] P. Knapp *et al.*, Bull. Am. Phys. Soc. **55**, 89 (2010).
[15] V. V. Ivanov *et al.*, Phys. Rev. E **79**, 056404 (2009).
[16] P. Wiewior *et al.*, J. Phys. Conf. Ser. **244**, 032013 (2010).
[17] V. V. Ivanov *et al.*, Phys. Rev. Lett. **100**, 025004 (2008).
[18] J. J. MacFarlane *et al.*, High Energy Density Phys. **3**, 181 (2007).
[19] S. V. Lebedev *et al.*, Phys. Rev. Lett. **85**, 98 (2000).
[20] V. V. Ivanov *et al.*, Phys. Rev. Lett. **97**, 125001 (2006).
[21] U. Andiel *et al.*, Rev. Sci. Instrum. **74**, 2369 (2003).
[22] F. J. Marshall *et al.*, Rev. Sci. Instrum. **77**, 10F308 (2006).
[23] E. Louzon *et al.*, J. Opt. Soc. Am. B **26**, 959 (2009).
[24] J. P. Chittenden and C. A. Jennings, Phys. Rev. Lett. **101**, 055005 (2008).